Microscopic theory of spin-polarization coupling in multiferroic transition metal oxides

Chenglong Jia,[1] Shigeki Onoda,[2] Naoto Nagaosa,[3,4] and Jung Hoon Han[5,6,*]

[1]*School of Physics, Korea Institute for Advanced Study, Seoul 130-012, Korea*

[2]*RIKEN (The Institute of Physical and Chemical Research), Wako 351-0918, Japan*

[3]*CREST, Department of Applied Physics, University of Tokyo, Tokyo 113-8656, Japan*

[4]*Correlated Electron Research Center, National Institute of Advanced Industrial Science and Technology, 1-1-1, Higashi, Tsukuba 305-8562, Japan*

[5]*BK21 Physics Research Division, Department of Physics, Sungkyunkwan University, Suwon 440-746, Korea*

[6]*CSCMR, Seoul National University, Seoul 151-747, Korea*

A systematic microscopic theory of magnetically induced ferroelectricity and lattice modulation is presented for various electron configurations of Mott-insulating transition metal oxides. The origin of polarization is classified as the spin-orbit interaction effective (i) within the magnetic t_{2g} orbitals, (ii) between the t_{2g} and e_g orbitals, and (iii) within the ligand ion's p orbitals. Predictions for x-ray and neutron scattering experiments are proposed to clarify the microscopic mechanism of the spin-polarization coupling in different materials. Semi-quantitative agreements with the multiferroic TbMnO$_3$ are obtained.

I. INTRODUCTION

The coupling among the charge, spin, and orbital degrees of freedom in Mott insulators has been one of the central issues in strongly correlated electron systems. Despite the localization of charge in Mott insulators, its displacement and the associated lattice deformation can be produced by a nontrivial low-energy magnetic and/or orbital structure, resulting in ferroelectric behavior. The ferroelectricity and the magnetism sometimes appear concomitantly in a class of Mott insulators known as the multiferroics.[1–3] Recently, a prototype of ferroelectricity associated with the spiral magnetic order has been found in TbMnO$_3$,[4] attracting revived interests in multiferroic behavior.[3] Now, the number of multiferroic materials has rapidly increased to include such wide diversity of Mott-insulating d-electron configurations as found in Ni$_3$V$_2$O$_8$,[5] Ba$_{0.5}$Sr$_{1.5}$Zn$_2$Fe$_{12}$O$_{22}$,[6] CoCr$_2$O$_4$,[7] MnWO$_4$,[8] CuFeO$_2$,[9] LiCuVO$_4$,[10] and LiCu$_2$O$_2$.[11] It is by now highly desirable that a systematic and quantitative microscopic description of the coupling between the magnetism and the electric dipole moment in *realistic* Mott-insulating electron configurations and a proper classification scheme of the multiferroic materials be established, which we undertake in this paper.

Theoretically, there are several possible mechanisms of magnetoelectric coupling already proposed. Usually, it is assumed that the largest magnetoelectric force is given by the exchange striction, which can give rise to the ferroelectric polarization when the inversion symmetry is broken.[2,12] On the other hand, a mechanism based on the spin-current picture has recently been proposed in which a local dipole moment can exist in proportion to $e \times (m_r \times m_{r+e})$, where m_r and m_{r+e} denote the local magnetic moments at sites r and $r+e$, respectively.[13–18] In this picture, a net electric polarization is found under spiral and conical spin structures. Yet another mechanism has been proposed for a model of t_{2g} electrons,[18] predicting induced dipole moments different from either the exchange striction or the spin-current mecha-

nism. In the latter two mechanisms, the spin-orbit interaction plays a crucial role, whereas the exchange striction does not depend on its existence. However, a coherent understanding is still missing for when and where each mechanism is active and dominant for the electric polarization of magnetic origin, which makes the systematic material design very difficult at the moment.

In this paper, we present a unified description of the magnetically induced polarization and lattice modulation in multiferroic transition metal oxides, by means of a perturbative expansion in both V/Δ and λ/Δ in generic Mott-insulating d-electron configurations. Here, V and Δ represent the hybridization and the charge transfer energy between the transition-metal (TM) d and ligand (L) p orbitals, and λ is the spin-orbit interaction energy. Spin-orbit interaction within the TM ion's t_{2g} orbitals and between the t_{2g} and e_g orbitals is shown to give rise to the polarization of the spin-current form. With e_g orbitals, the spin-orbit interaction at the ligand ionic site is argued to provide an important mechanism of spin-polarization coupling. A classification scheme is offered for the induced polarization (Table I), which should serve to identify the dominant magnetoelectric mechanism by probing the nonuniform shifts of the L ions using x-ray and neutron scattering.

TABLE I. Wave vectors and directions of the lattice modulation originating from the mechanisms P^{ms}, P^{orb}, and P^{sp}.

$P(q)$	Mechanisms	Polarization
$P(0)$	P^{sp}	$-e \times (m_1 \times m_2) \sin Q \cdot e$
$P(\pm(\pi e + Q))$	P^{ms}	$e[m_0 \cdot (m_1 \pm im_2)] \cos[Q \cdot e/2]$
$P[\pm(\pi e + 2Q)]$	P^{ms}	$e(m_1^2 + m_2^2)/4$
$P(\pm Q)$	P^{orb}	$\mp i[(e \cdot m_0)m_\pm + (e \cdot m_\pm)m_0]$
	P^{sp}	$\mp \frac{i}{2} e \times (m_0 \times m_\mp) \sin[Q \cdot e/2]$
$P(\pm 2Q)$	P^{orb}	$\mp \frac{i}{2}[(e \cdot m_\pm)m_\pm] \sin Q \cdot e$
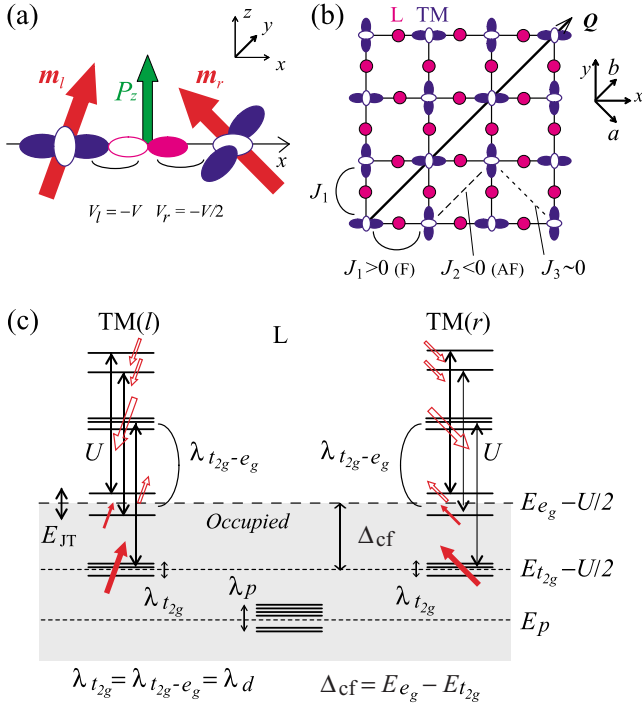
FIG. 1. (Color online) (a) The TM-*L*-TM cluster model with the rod-type $d_{3x^2-r^2}/d_{3y^2-r^2}$ staggered orbital order under a noncollinear spin configuration ($\boldsymbol{m}_l$ and $\boldsymbol{m}_r$) with the associated electric polarization P_z. V_l and V_r denote the pd hybridization. (b) The lattice structure and the staggered orbital order of TbMnO$_3$ within the xy (or ab) plane. (c) The level scheme for the $t_{2g}^3 e_g^1$ high-spin ($S=2$) configuration.

Discussion of the spin-induced polarization in various circumstances can be found in Sec. II, along with a cluster model on which the derivation of the spin-polarization coupling is based. As the specific demonstration of the various mechanisms at work, key experimental observations on the polarization and the lattice modulation in TbMnO$_3$ are explained within our scheme in Sec. III. We conclude with a summary and outlook in Sec. IV.

II. CLASSIFICATION OF MAGNETICALLY INDUCED POLARIZATION

A. Model

Let us consider a cluster composed of TM ions at $\boldsymbol{r}$ and $\boldsymbol{r}+\boldsymbol{e}$ hybridized through a L ion at the center $\boldsymbol{r}+\boldsymbol{e}/2$, as shown in Fig. 1(a). For simplicity, we neglect a deviation of the bond angle away from 180°. The dipole moment $\boldsymbol{P}_{\boldsymbol{r}+\boldsymbol{e}/2}$ induced at the ligand site $\boldsymbol{r}+\boldsymbol{e}/2$ is given by the general expression

$$\boldsymbol{P}_{\boldsymbol{r}+\boldsymbol{e}/2} = P^{\mathrm{ms}}(\boldsymbol{m}_{\boldsymbol{r}} \cdot \boldsymbol{m}_{\boldsymbol{r}+\boldsymbol{e}})\boldsymbol{e} + P^{\mathrm{sp}}\boldsymbol{e} \times (\boldsymbol{m}_{\boldsymbol{r}} \times \boldsymbol{m}_{\boldsymbol{r}+\boldsymbol{e}})$$
$$+ P^{\mathrm{orb}}[(\boldsymbol{e} \cdot \boldsymbol{m}_{\boldsymbol{r}})\boldsymbol{m}_{\boldsymbol{r}} - (\boldsymbol{e} \cdot \boldsymbol{m}_{\boldsymbol{r}+\boldsymbol{e}})\boldsymbol{m}_{\boldsymbol{r}+\boldsymbol{e}}], \quad (2.1)$$

up to second order in the local spin moments $\boldsymbol{m}_{\boldsymbol{r}}$ and $\boldsymbol{m}_{\boldsymbol{r}+\boldsymbol{e}}$, taken to have the unit magnitude $|\boldsymbol{m}_{\boldsymbol{r}}|=1$ everywhere. The case with nonuniform magnetic moment size can be treated using the technique described later in the paper. There can be

polarizations of nonmagnetic origin that we will omit in the discussion.

In the above formula, $P^{\mathrm{ms}} \propto (V/\Delta)^3$ is the magnetostriction, which does not depend on the spin-orbit interaction. The spin-current term $P^{\mathrm{sp}} \propto (\lambda/\Delta)(V/\Delta)^3$ and the orbital term $P^{\mathrm{orb}} \sim \min(\lambda/V,1)(V/\Delta)$ have been obtained in the study of partially filled, degenerate t_{2g} orbitals.[13,18] Further investigation carried out in this paper shows that P^{sp} is present for generic Mott-insulating d-electron configurations with nonzero local moments, whereas P^{orb} is only found for partially filled t_{2g} systems.

Equation (2.1) can be derived from the TM-L-TM cluster model[13,18] composed of the L p orbitals and the two TM d orbitals, which are coupled with L through the hybridization integrals $V_{pd\sigma}$ and $V_{pd\pi}$ corresponding to σ and π bonding of the orbitals, respectively. The TM d levels are assumed to be split by the crystal field into t_{2g} and e_g orbitals with the respective local energy levels given by $E_{t_{2g}}$ and E_{e_g}, while the L p orbitals are assumed degenerate with the energy E_p. The spin-orbit couplings for d and p orbitals are given by λ_d and λ_p, respectively. Finally, an effective Zeeman field $(U/2)\hat{\boldsymbol{m}}_a$ ($a=l/r$ for the left/right TM ion) with an energy separation U is assumed, which originates from the local Coulomb repulsion and Hund's-rule coupling in the magnetically ordered phase. Our model Hamiltonian thus reads $H = H_d + H_p + H_{dp} + H_{so}$, where

$$H_d = -\frac{U}{2} \sum_{a=l,r} \sum_{\alpha} \boldsymbol{m}_a \cdot \boldsymbol{s}_{a\alpha},$$

$$H_p = E_p \sum_{\beta\sigma} p_{\beta\sigma}^+ p_{\beta\sigma},$$

$$H_{dp} = \sum_{a=l,r} \sum_{\sigma\alpha\beta} V_{a\alpha\beta}(d_{a\alpha\sigma}^+ p_{\beta\sigma} + \mathrm{H.c.}). \quad (2.2)$$

Here, α and β refer to the d and p orbitals involved in the hybridization, respectively. Particle-hole transformations, $d_{a\alpha\sigma} \rightarrow \sigma d_{a\alpha\bar{\sigma}}^+$ and $p_{\beta\sigma} \rightarrow \sigma p_{\beta\bar{\sigma}}^+$ ($\bar{\sigma} \equiv -\sigma$), have been implemented on both the p and d orbitals. The local field direction is given by $\boldsymbol{m}_a = (\sin\theta_a\cos\phi_a, \sin\theta_a\sin\phi_a, \cos\theta_a)$ for left (l) and right (r) d-electron sites, and $\boldsymbol{s}_{a\alpha}$ is the spin operator of the d-orbital state α. The hybridization matrix $V_{a\alpha\beta}$ depends on the d and p orbitals involved (corresponding to σ and π bonding of the orbitals) and also on their relative positions (left or right). The spin-orbit interaction H_{so} can be imposed either for the magnetic d orbitals or the ligand ion p orbitals. The polarizations that result from each case are the subject of discussion in the following sections.

A projection scheme in which the spin orientation antiparallel to the local Zeeman field is truncated out was introduced in Ref. 18 and is used throughout this paper as well. The scheme will be explained again when we consider the case of active e_g orbitals below.

On a linear array of $\cdots$-TM-L-TM-$L$$\cdots$, the various mechanisms of polarization included in Eq. (2.1) are manifested as Fourier harmonics in x-ray or neutron scattering probes. Assuming a general conical structure $\boldsymbol{m}_{\boldsymbol{r}} = \boldsymbol{m}_0 + \boldsymbol{m}_1\cos\boldsymbol{Q}\cdot\boldsymbol{r} - \boldsymbol{m}_2\sin\boldsymbol{Q}\cdot\boldsymbol{r}$, we obtain the nontrivial Fourier

TABLE II. Classification of the relevant orbitals coupled by the spin-orbit interaction, the d-electron configuration, the corresponding types of induced polarization, and the materials in which the polarization mechanism is expected to be active.

Orbitals	Configuration	Polarization	Materials
t_{2g}	t_{2g}^n ($n=1,2,4,5$)	P^{sp}, P^{orb}	Ref. 19
p	Arbitrary d^n, nonzero S	P^{sp}	Refs. 4–6 and 8–11
t_{2g}-e_g	Arbitrary d^n, nonzero S	P^{sp}	Refs. 4 and 6–9

components $P(q) = \Sigma_{r,e} P_{r+e/2} e^{-iq \cdot (r+e/2)}$ shown in Table I, with $m_{\pm} = m_1 \pm im_2$ and $P_{r+e/2}$ given in Eq. (2.1). We allowed for the general case of (up to) two inequivalent L positions due to, for instance, the orthorhombic distortion and/or staggered orbital order in establishing Table I. To compensate the electrostatic energy loss, each L ion tends to shift toward the induced dipole moment and cause the lattice modulation with the same wave vectors.

P^{ms} gives a collinear lattice modulation along the cluster direction with wave vectors $\pi e + Q$ and $\pi e + 2Q$, where the shift of πe is due to the presence of two equivalent L sites. This case is relevant for $HoMnO_3$ as pointed out by Sergienko and Dagotto recently.[16] Under the spiral (conical) magnetic structure, P^{orb} yields a spiral, even noncoplanar, modulation, while P^{sp} gives a uniform (conical) modulation. P^{orb} is found only in the unquenched t_{2g} system.[18] Under the spiral magnetic structure, P^{orb} gives the spiral modulation at twice the magnetic wave vector. The induced dipole moment contains both oscillating and uniform components, but the macroscopic polarization is due only to P^{sp} or P^{ms} for the special case with the four periodicity $Q \cdot e = \pi/2$.[16] Table I can be used to classify the mechanisms of the magnetoelectric couplings using x-ray and neutron scattering experiments.

The mechanisms responsible for the spin-induced dipole moments through spin-orbit coupling can be classified as in Table II. We have identified three mechanisms that contribute to the magnetically induced polarization, in the absence of the lattice symmetry breaking. They are mediated by the spin-orbit interactions active (i) within the t_{2g} orbitals, (ii) within the L p orbitals, and (iii) within the magnetic ions and which couples the $t_{2g}-e_g$ orbitals. In the following sections, we describe each of the mechanisms in detail.

B. t_{2g}-orbital mixing by spin-orbit interaction

Spin-orbit interaction within the degenerate t_{2g} manifold (intra-t_{2g}) produces polarizations, P^{sp} and P^{orb},[13,18] for t_{2g}^n with the electron number $n=1,2,4,5$. As shown in a previous paper,[18] P^{orb} and P^{sp} appear in proportion to $\min(\lambda_d/V_{pd\pi},1)(V_{pd\pi}/\Delta)$ and $(\lambda_d/\Delta)(V_{pd\pi}/\Delta)$,[3] with $\Delta = E_{t_{2g}} \pm U/2 - E_p$. Here, the $\pm$ sign in Δ refers to the charge transfer energy from the filled L site to the t_{2g} orbital in the t_{2g}^5 and t_{2g}^2 configurations, respectively.

Numerical solution of the cluster model yielded similar results for t_{2g}^1 and t_{2g}^4 configurations. The t_{2g}^3 and t_{2g}^6 configu-

rations represent the orbital-quenched case with no polarization arising from intra-t_{2g} spin-orbit interaction. Even in this case, mixing with the unoccupied e_g orbitals due to the spin-orbit interaction, to be discussed later, can result in the orbital deformation and the induced dipole moment.[7] Another symmetry operation can be used to show that P^{sp} and P^{orb} for t_{2g}^4 are related to those of t_{2g}^5 by a sign change, as well as those for t_{2g}^1 to t_{2g}^2.

A low-n transition metal involving Ti or V will be the likely candidate to observe t_{2g}-mediated P^{sp} and P^{orb}. A spin-canted phase in YVO_3 was found recently.[19] For such a state, we argue that P^{orb}, which is much larger than P^{sp} on the atomic scale, is detectable in the microscopic x-ray or neutron probes and can be compared with the expressions given in Eq. (2.1) and Table I.

C. p-orbital mixing by spin-orbit interaction

A number of e_g systems with filled t_{2g} came to be classified as a multiferroic: $Ni_3V_2O_8$ (Ref. 5) with the d-orbital configuration $t_{2g}^6 e_g^2$ and $LiCuVO_4$ (Ref. 10) and $LiCu_2O_2$ (Ref. 11) both with $t_{2g}^6 e_g^3$. The two orbital states comprising the e_g level differ by two units of angular momentum l_z ($l_z = 0, \pm2$), whereas the spin-orbit interaction only connects states with angular momentum mismatch of 1. Therefore, the spin-orbit interaction within the e_g manifold vanishes. Bearing this in mind, we propose that the oxygen spin-orbit-mediated mechanism,

$$H_{so}^p = \lambda_p \hat{L}_p \cdot \hat{S}_p, \qquad (2.3)$$

should play an important role for these materials. Here, $\hat{L}_p$ and $\hat{S}_p$ schematically refer to the angular momentum and spin operators of the p orbitals.

For instance, the d^9 Cu sites can be modeled as $d_{x^2-y^2}$ orbitals at the TM sites in the cluster model. Taking the hybridization to the left (V_l) and the right (V_r) TM ions to be $-V_l = V_r = V_{pd\sigma}$ [see Fig. 1(a)], the resulting polarization P^{sp} mediated by the oxygen spin-orbit interaction is given by (details in Appendix A)

$$P_p^{sp} = -4\sqrt{2} L_{x^2-y^2,z}^z \frac{\lambda_p}{\Delta} \left(\frac{V_{pd\sigma}}{\Delta} \right)^3. \qquad (2.4)$$

Here, E_{e_g} is the energy of the $d_{x^2-y^2}$ orbital, $\Delta = E_{e_g} + U/2 - E_p$, and $L_{x^2-y^2,z}^z = \langle d_{x^2-y^2}|z|p_z \rangle$.

The d^8 contains two e_g orbitals with the total spin $S=1$, which can be decomposed as $d_{3x^2-r^2}$ and $d_{y^2-z^2}$ in the degenerate case. Of these, the latter does not couple to the oxygen orbitals and one is left with a single $d_{3x^2-r^2}$ orbital per site with the polarization again given by Eq. (2.4) with the $d_{3x^2-r^2}$ replacing $d_{x^2-y^2}$. No P^{orb} term is found for pure e_g models with the oxygen spin-orbit interaction.

The d^7 case with a single e_g electron is subject to the Jahn-Teller (JT) distortion and the lifting of the orbital degeneracy. When the adjacent TM sites are occupied by the same e_g orbitals due to the JT distortion, one again has Eq. (2.4). If not, the appropriate cluster model should involve different orbitals for the right and left TM's, and the inver-

sion symmetry breaking yields nonzero values of P^{ms}. On the local scale, P^{ms} is greater than P_p^{sp}, but its macroscopic average usually vanishes. Although analytical expressions for the induced dipole moment is not available in this case, our numerical study confirms that the dependence of the induced polarization on the magnetic moment orientations is always given by Eq. (2.1). Both constants, P^{ms} and P_p^{sp}, can be worked out numerically.

D. t_{2g}-e_g-orbital mixing by spin-orbit interaction

In addition to the intra-t_{2g} and intra-p-orbital spin-orbit interactions discussed above, mixing of an occupied e_g and an unoccupied t_{2g} orbital, or of an unoccupied e_g and an occupied t_{2g}, can occur due to the spin-orbit interaction,

$$H_{so}^{t_{2g}-e_g} = \lambda_d \hat{L}_d \cdot \hat{S}_d, \qquad (2.5)$$

within a given TM ion and contribute to the polarization P^{sp}.[17] An earlier consideration[13,18] restricted the effect of the above spin-orbit Hamiltonian within the t_{2g} subspace. Here, we focus on the matrix elements connecting the t_{2g} and the e_g orbitals through spin-orbit coupling and demonstrate the effect of the t_{2g}-e_g mixing on the induced polarization within the cluster model. In particular, the case of Mn^{3+} ions in TbMnO$_3$ is studied as the prototype case.

The Mn^{3+} ions in TbMnO$_3$ have the $t_{2g}^3 e_g^1$ configuration. Because of the large Jahn-Teller effect, TbMnO$_3$ exhibits the rod-type $d_{3x^2-r^2}/d_{3y^2-r^2}$ orbital ordering shown in Fig. 1(b) far above the room temperature.[20] Accordingly, we assume that the $d_{3x^2-r^2}$ and $d_{3y^2-r^2}$ orbitals are occupied at the l and r sites of the TM-L-TM cluster. Assuming $V_l = V_r = -V_{pd\sigma}$, one obtains polarization of the spin-current form, due to the t_{2g}-e_g mixing (see Appendix B),

$$P_{t_{2g}-e_g}^{sp} = -\sqrt{3} L_{zx,x}^z \frac{\lambda_d}{U - \Delta_{cf} + E_{JT}/2} \left(\frac{V_{pd\sigma}}{\Delta} \right)^3, \qquad (2.6)$$

where Δ_{cf} is the crystal field gap $E_{e_g} - E_{t_{2g}}$, E_{JT} is the Jahn-Teller energy splitting, and $L_{zx,x}^z = \langle d_{zx} | z | p_x \rangle$. A similar term is obtained in the case of uniform orbital order, i.e., same d orbitals for both TM ions in the cluster. We expect the t_{2g}-e_g mixing mechanism to be operative for arbitrary d^n configurations. Particularly the high-spin state of Fe^{3+} (d^5, $S = 5/2$) where the orbital angular momentum is supposed to be quenched, the t_{2g}-e_g spin-orbit interaction could give a fairly large polarization. The GdFeO$_3$-type orthorhombic distortion present in perovskite oxides could also mix t_{2g} and e_g orbitals and contribute to the polarization. This distortion also increases the intra-t_{2g} contribution to the P^{sp} due to the larger matrix element $L_{zx,x}^z$, which is now allowed in addition to the rather small $L_{yz,y}^z = \langle d_{yz} | z | p_y \rangle$ for cubic perovskites.[13,18] No orbital polarization P^{orb} is induced from the mixing. The three mechanisms of generating local dipole moment from the magnetic order, intra-t_{2g}, intra-p, and t_{2g}-e_g mixing, are summarized in Table II.

In addition to TbMnO$_3$, the t_{2g}-e_g mixing should play a prominent role in other multiferroic materials discussed in Refs. 6–9. Quite remarkably, the spin-current mechanism of the polarization is found for all three cases: intra-t_{2g}, intra-p, and t_{2g}-e_g mixed. The three mechanisms are summarized in Table II.

III. COMPARISON TO EXPERIMENTS

In this section, a semiquantitative analysis based on the above theory is given to explain the experiments in TbMnO$_3$, where the simultaneous presence of orbital ordering, unfilled e_g levels, and t_{2g}-e_g mixing presents a complex challenge for theory. The two terms, Eqs. (2.4) and (2.6), combine constructively to produce P^{sp}, the uniform polarization. Quantitative agreement with the measured uniform polarization value in TbMnO$_3$ is obtained as follows.

Matrix elements needed to evaluate Eqs. (2.4) and (2.6) are calculated by taking the TM–O bond length 1.9 Å and the Clementi-Raimondi effective charges[21] $Z_{Mn\,3d}^{eff} = 10.53$ and $Z_{O\,2p}^{eff} = 4.45$. Other parameters are chosen as $V_l = 2V_r = -V_{pd\sigma} = -1.2$ eV, $U = 3$ eV, and $E_{e_g} - E_p = 2$ eV. The spin-orbit coupling for the oxygen $2p$ and TM $3d$ orbitals are chosen as $\lambda_p = 25$ meV and $\lambda_d = 48$ meV from $\lambda_L \equiv 2\Delta E_L/(2L+1)$, where $L = 1, 2$ for p and d orbitals. The spin-orbit energy splitting is given by $\Delta E_p = 37$ meV ($\lambda_p = 25$ meV) and $\Delta E_d = 120$ meV ($\lambda_d = 48$ meV).[22]

With these values, we obtain the uniform polarization along the c axis $P_p^{sp} \sim 130$ μC/m^2 from the oxygen spin-orbit interaction and $P_{t_{2g}-e_g}^{sp} \sim 860$ μC/m^2 from the t_{2g}-e_g mixing with $\Delta_{cf} = 2$ eV and $E_{JT} = 1$ eV. The net value $P^{sp} \sim 990$ μC/m^2 multiplied with $|\mathbf{m}_r \times \mathbf{m}_{r+e}| \approx \sin(0.28\pi)$ in Eq. (2.1) gives the uniform c-axis polarization of ~ 760 μC/m^2, in reasonable agreement with the experimental value in TbMnO$_3$ (Ref. 4) (~ 700 μC/m^2 at 10 K). The direction of the polarization is also consistent with the experiment.

Another interesting aspect of TbMnO$_3$ concerns the x-ray intensity of the $2Q$ lattice modulation, which increases monotonically in the temperature range T_N (onset of the collinear magnetic phase) and T_L (onset of spiral magnetic order), then decreases upon lowering the temperature.[4] The spin configuration in the magnetic phase $T < T_N$ can be described by the ordered spin moment, $\langle \mathbf{s}_i \rangle = S(\hat{b} \cos \theta_i + \hat{c}\sqrt{1-e^2} \sin \theta_i)$, where θ_i evolves roughly with the period of seven lattice constants. The collinear phase can be modeled with $e = 1$ and the magnitude S increasing monotonically at the lower temperature. The elliptic spiral phase below T_L evolves from collinear ($e = 1$) to nearly circular ($e = 0$) pattern with decreasing temperature,[4] while S remains more or less constant. In both instances, the size of the local magnetic moment $|\langle \mathbf{s}_i \rangle|$ depends on the coordinate. The TM-L-TM cluster calculation, originally for equal magnetic moment sizes on the TM ions, can be generalized to handle the nonuniform cases by writing a self-consistent equation,

$$\langle \mathbf{s}_i \rangle = \frac{\int d\Omega_i \mathbf{m}_i w_i}{\int d\Omega_i w_i}, \qquad (3.1)$$

with a Boltzmann-like weight $w_i = \exp[\beta_i \langle \mathbf{s}_i \rangle \cdot \mathbf{m}_i]$. Here, the self-consistent parameter β_i (not to be confused with the in-

FIG. 2. (Color online) (a) Elliptic spiral spins (arrows at magnetic M ions) with the ellipticity $e=0.6$ and the associated local dipole moments (at oxygen O sites) arising from oxygen spin-orbit interaction are shown as P_z^{sp} (along the z direction, enlarged by 10^3 times) and P_x^{ms} (along the x direction) for the observed spin modulation period ($Q \approx 0.28\pi$) as in TbMnO$_3$ at low temperature. Two types of M sites exist (even and odd i) due to the orbital ordering. Statistical weights are introduced to account for elliptic spins. P_x^{ms} alternates its direction due to the staggered orbital order. (b) Induced dipole moments $P_{z,i}^{sp}$ and $|P_{x,i}^{ms}|$ at the oxygen site O$_i$ in TM$_i$-O$_i$-TM$_{i+1}$ cluster in units of $10^{-3}L_z$ and $10^{-3}L_x$, respectively, with $L_z = \langle d_{zx}|z|p_x \rangle$ and $L_x = \langle d_{3x^2-r^2}|x|p_x \rangle$. [(c) and (d)] Main Fourier components of the dipole moments, at $q=2Q$ for $|P_x^{ms}|$ and at $q=0$ for $P_{z,i}^{sp}$, as functions of e for $T<T_L$ in (c) and S with $e=1$ for $T_L<T<T_N$ in (d). Note that e in (c) and $1/2-S$ in (d) decrease with decreasing temperature. This figure is worked out for the orbital ordered model of TbMnO$_3$ (Fig. 1) with $(U,\Delta_{cf},E_{JT},V_{pd\sigma},\lambda_p,\lambda_d)=(3.0,2.0,1,1.2,0.025,0.048)$ eV.

verse temperature) is used to produce the desired average magnetic moment at each site i by averaging over the $O(3)$ unit vector $\mathbf{m}_i$. The dipole moment at $r+e/2$ in the collinear and/or elliptic spin configuration can be obtained by taking the average of Eq. (2.1) over the spins $\mathbf{m}_r$ and $\mathbf{m}_{r+e}$ with weights w_r and w_{r+e}, using $\langle \mathbf{s}_i \rangle$ for the spin configuration of the low-temperature TbMnO$_3$. According to our classification scheme (Table I), P^{ms} is the only mechanism operative at the wave vector $2Q$.

As shown in Figs. 2(c) and 2(d), the increasing signal in the collinear phase, followed by the decrease in the noncollinear phase in the $2Q$ intensity, arising from the magnetostriction P^{ms}, is consistent with the experiment. The direction of the lattice modulation is predicted to be along the $\hat{b}$ axis while experimentally it has not been clearly determined yet.[23] A proper identification of the lattice modulation direction in the future will be essential to discriminate the different scenarios of magnetoelectric coupling.

IV. CONCLUSIONS

We have presented a complete identification of the mechanisms responsible for magnetically induced polarization in the TM-L-TM$\cdots$ array using the cluster model.[24] The driving force is the spin-orbit interaction active either in the magnetic or the ligand ions. Three mechanisms are considered in this work: polarization driven by spin-orbit mixing of t_{2g} orbitals, of p orbitals when the t_{2g} orbital is quenched, and finally of t_{2g}-e_g mixing. In agreement with the polarization observed in the spiral magnetic phase over a wide vari-

ety of multiferroic materials in recent years, our consideration leads to the spin-current form of induced polarization regardless of the mechanisms considered. Sometimes there can be more than one source of polarization, such as due to both oxygen-mediated and t_{2g}-e_g mixing-mediated polarizations in TbMnO$_3$. In such cases, the various contributions must add up to give the polarization in real materials. A good quantitative agreement with the observed polarization value in TbMnO$_3$ has been obtained in this way.

There are other induced polarizations with nonzero modulation wave vectors that we have identified. The classification scheme presented here will be of help in identifying and classifying the origin of spin-induced polarization in future multiferroic research.

APPENDIX A: THE DIPOLE MOMENTS INDUCED BY OXYGEN SPIN-ORBIT INTERACTION

In this appendix, we calculate the dipole moment induced at the oxygen site by deriving the ground state in terms of the strong-coupling expansion in terms of V/U and taking the expectation value of the position r operator. First, due to the large energy difference U separating the parallel and antiparallel d states, we diagonalize H_d for the e_g^1 configuration by using the low-energy d_a orbital operator,[18]

$$d_a^+ = \cos(\theta_a/2)d_{a\uparrow}^+ + e^{-i\phi_a}\sin(\theta_a/2)d_{a\downarrow}^+. \quad (A1)$$

at the site $a=l,r$. For H_p, with the spin-orbit interaction H_{so}^p acting on the local p orbitals, the six p states are splitted into four with the total angular momentum $J=3/2$ and two with $J=1/2$. Of these, only the following four contain the p_x orbital and hybridize with the e_g levels, $\mathcal{P}_1^+=\sqrt{\frac{2}{3}}p_{x\uparrow}^+ + \frac{1}{\sqrt{3}}p_{1\downarrow}^+$, $\mathcal{P}_2^+=\sqrt{\frac{2}{3}}p_{x\downarrow}^+ + \frac{1}{\sqrt{3}}p_{1\uparrow}^+$, $\mathcal{P}_3=\frac{1}{\sqrt{3}}p_{x\uparrow}^+ - \sqrt{\frac{2}{3}}p_{1\downarrow}$, and $\mathcal{P}_4^+=\frac{1}{\sqrt{3}}p_{x\downarrow}^+ - \sqrt{\frac{2}{3}}p_{1\uparrow}^+$. Here, $1(\bar{1})$ refers to the p-orbital angular momentum. The remaining two p orbitals are left out as they are completely decoupled from the others. In diagonalizing H_{dp}, it is convenient to use an orthonormal basis given by

$$\begin{pmatrix} Q_{1,2}^+ \\ Q_{3,4}^+ \end{pmatrix} = \frac{1}{\sqrt{2(1 \pm |\kappa|)}}\left[\begin{pmatrix} P_2^+ \\ P_4^+ \end{pmatrix} \pm e^{i\eta}\begin{pmatrix} P_1^+ \\ P_3^+ \end{pmatrix} \right], \quad (A2)$$

where $P_{2i-1,2i}=\cos(\theta_{l,r}/2)\mathcal{P}_{2i-1}+e^{i\phi_{l,r}}\sin(\theta_{l,r}/2)\mathcal{P}_{2i}$ for $i=1,2$. Nonorthogonality of (P_1,P_2) and (P_3,P_4) pairs leads to the overlap $\kappa=\langle 0|P_1P_2^+|0\rangle=\langle 0|P_3P_4^+|0\rangle$ and $e^{i\eta}=\kappa/|\kappa|$. After redefining $d_a'=\text{sgn}[V_a]d_a$, and introducing

$$D^+_{1,2} = \frac{1}{\sqrt{2}}(d'^+_r \pm e^{i\eta}d'^+_l), \tag{A3}$$

the effective Hamiltonian for the symmetric case $|V_l|=|V_r| =V$ is written as $[\Psi^T_m=(D_m, Q_m, Q_{m+2})]$

$$H = \sum_{m=1,2} \Psi^+_m \begin{pmatrix} -U/2 & V_m & V'_m \\ V_m & E'_p & 0 \\ V'_m & 0 & E''_p \end{pmatrix} \Psi_m, \tag{A4}$$

where $V_{1,2}=V\sqrt{(1\pm|\kappa|)/3}$, $E'_p=E_p+\lambda_p/2$, and $E''_p=E_p-\lambda_p$. In the energy hierarchy of our interest, the two lowest $E_{m1}\approx -U/2$ (hole) states will be occupied first, and the dipole moment $\mathbf{P}=\Sigma_{m=1,2}\langle X_{m1}|\mathbf{r}|X_{m1}\rangle$ is calculated,

$$P^{sp}_p = -2\sqrt{2}(L^z_{rz}+L^z_{lz})\frac{\lambda_p}{\Delta}\left(\frac{V}{\Delta}\right)^3 \hat{x}\times(\mathbf{m}_l\times\mathbf{m}_r),$$

$$P^{ms} = -\frac{1}{4}(L^x_{rx}-L^x_{lx})\left(\frac{V}{\Delta}\right)^3\hat{x}(\mathbf{m}_l\cdot\mathbf{m}_r), \tag{A5}$$

with $\Delta=E_{e_g}+U/2-E_p$. Here, L^z_{az} (L^x_{ax}) are the nonzero overlap integrals between e_g d orbital and oxygen p_z (p_x) orbitals, $L^z_{az}=\langle d_a|z|p_z\rangle$ and $L^x_{ax}=\langle d_a|x|p_x\rangle$ with $a=l(r)$, respectively. Note that if the identical orbitals are positioned on either side of the oxgen, such as d^9 Cu with $d_{x^2-y^2}$, P^{ms} will vanishe and P^{sp}_p reduces to Eq. (2.4).

APPENDIX B: MECHANISM OF t_{2g}-e_g MIXING

As shown in Fig. 1(c), the occupied e_g and the unoccupied t_{2g} orbitals are separated by the energy gap $\Delta'=U-\Delta_{cf}+E_{JT}/2$; taking bare Hamiltonian of the e_g levels as

$$H^a_d = \Delta'\sum_\sigma (d^+_{a,x^2-y^2\sigma}d_{a,x^2-y^2\sigma} + d^+_{a,3z^2-r^2\sigma}d_{a,3z^2-r^2\sigma}),$$
$$\tag{B1}$$

with $a=1,r$ and we treat $H^{t_{2g}-e_g}_{so}$ perturbatively. For Mn^{3+} ions, since all parallel t_{2g} states are already occupied by electrons, we can furthermore truncate out these components.

Then, the perturbed e_g states are given by the first-order perturbation theory,

$$|d_{a,x^2-y^2\uparrow}\rangle' = |d_{a,x^2-y^2\uparrow}\rangle + \frac{\lambda_d}{\Delta'}\left(-ie^{i\phi_a}\sin\frac{\theta_a}{2}|d_{a,xy}\rangle\right.$$
$$\left. + \frac{1}{2}\cos\frac{\theta_a}{2}(|d_{a,zx}\rangle - i|d_{a,yz}\rangle)\right)|AP_a\rangle,$$

$$|d_{a,x^2-y^2\downarrow}\rangle' = |d_{a,x^2-y^2\downarrow}\rangle + \frac{\lambda_d}{\Delta'}\left(-i\cos\frac{\theta_a}{2}|d_{a,xy}\rangle\right.$$
$$\left. + \frac{1}{2}e^{i\phi_a}\sin\frac{\theta_a}{2}(|d_{a,zx}\rangle + i|d_{a,yz}\rangle)\right)|AP_a\rangle,$$

$$|d_{a,3z^2-r^2\uparrow}\rangle' = |d_{a,3z^2-r^2\uparrow}\rangle - \frac{\lambda_d}{\Delta'}\frac{\sqrt{3}}{2}\cos\frac{\theta_a}{2}[|d_{a,zx}\rangle + i|d_{a,yz}\rangle]$$
$$\times|AP_a\rangle,$$

$$|d_{a,3z^2-r^2\downarrow}\rangle' = |d_{a,3z^2-r^2\downarrow}\rangle - e^{i\phi_a}\sin\frac{\theta_a}{2}\frac{\lambda_d}{\Delta'}\frac{\sqrt{3}}{2}[|d_{a,zx}\rangle - i|d_{a,yz}\rangle]$$
$$\times|AP_a\rangle. \tag{B2}$$

Here, the substitutions, $|\uparrow\rangle\rightarrow -e^{i\phi_a}\sin(\theta_a/2)|AP_a\rangle$ and $|\downarrow\rangle\rightarrow\cos(\theta_a/2)|AP_a\rangle$, have been used to describe the spin state of the antiparallel unoccupied t_{2g} orbitals.

Now, the Mn^{3+} ions on the left and the right are described by $|d_{l,3x^2-r^2}\rangle' = -\frac{1}{2}|d_{l,3z^2-r^2}\rangle' + \frac{\sqrt{3}}{2}|d_{l,x^2-y^2}\rangle'$ and $|d_{r,3y^2-r^2}\rangle' = -\frac{1}{2}|d_{r,3z^2-r^2}\rangle' - \frac{\sqrt{3}}{2}|d_{r,x^2-y^2}\rangle'$ orbitals, respectively. Both are hybridized with the oxygen p_x orbital. The effects of spin-orbit interaction is already included in the modified wave functions given in Eq. (B2). Then, the model Hamiltonian [Eq. (2.2)] can be easily diagonalized by using the techinques developed in Appendix A, which leads to the polarization in Eq. (2.6).

*hanjh@skku.edu

[1] P. Curie, J. Phys. (Paris), Colloq. **3**, 393 (1894).

[2] M. Fiebig, J. Phys. D **38**, R123 (2005).

[3] Y. Tokura, Science **312**, 1481 (2006).

[4] T. Kimura, T. Goto, H. Shintani, K. Ishizaka, T. Arima, and Y. Tokura, Nature (London) **426**, 55 (2003); M. Kenzelmann, A. B. Harris, S. Jonas, C. Broholm, J. Schefer, S. B. Kim, C. L. Zhang, S.-W. Cheong, O. P. Vajk, and J. W. Lynn, Phys. Rev. Lett. **95**, 087206 (2005); T. Arima, A. Tokunaga, T. Goto, H. Kimura, Y. Noda, and Y. Tokura, *ibid*. **96**, 097202 (2006).

[5] G. Lawes, A. B. Harris, T. Kimura, N. Rogado, R. J. Cava, A. Aharony, O. Entin-Wohlman, T. Yildrim, M. Kenzelmann, C. Broholm, and A. P. Ramirez, Phys. Rev. Lett. **95**, 087205 (2005).

[6] T. Kimura, G. Lawes, and A. P. Ramirez, Phys. Rev. Lett. **94**, 137201 (2005).

[7] Y. Yamasaki, S. Miyasaka, Y. Kaneko, J.-P. He, T. Arima, and Y. Tokura, Phys. Rev. Lett. **96**, 207204 (2006).

[8] K. Taniguchi, N. Abe, T. Takenobu, Y. Iwasa, and T. Arima, Phys. Rev. Lett. **97**, 097203 (2006).

[9] T. Kimura, J. C. Lashley, and A. P. Ramirez, Phys. Rev. B **73**, 220401(R) (2006).

[10] Y. Naito, Kenji Sato, Yukio Yasui, Yusuke Kobayashi, Yoshiaki Kobayashi, and Masatoshi Sato, arXiv:cond-mat/0611659 (unpublished).

[11] S. Park, Y. J. Choi, C. L. Zhang, and S.-W. Cheong, Phys. Rev. Lett. **98**, 057601 (2007).

[12] S. Greenwald and J. S. Smart, Nature (London) **166**, 523 (1950);

J. S. Smart and S. Greenwald, Phys. Rev. **82**, 113 (1951).

[13] H. Katsura, Naoto Nagaosa, and Alexander V. Balatsky, Phys. Rev. Lett. **95**, 057205 (2005).

[14] M. Mostovoy, Phys. Rev. Lett. **96**, 067601 (2006).

[15] A. B. Harris, T. Yildirim, A. Aharony, and O. Entin-Wohlman, Phys. Rev. B **73**, 184433 (2006).

[16] I. A. Sergienko and E. Dagotto, Phys. Rev. B **73**, 094434 (2006); I. A. Sergienko, Cengiz Sen, and Elbio Dagotto, Phys. Rev. Lett. **97**, 227204 (2006).

[17] C. D. Hu, arXiv:cond-mat/0608470 (unpublished).

[18] C. Jia, S. Onoda, N. Nagaosa, and J. H. Han, Phys. Rev. B **74**, 224444 (2006).

[19] Y. Ren, T. T. M. Palstra, D. I. Khomskii, E. Pellegrin, A. A. Nugroho, A. A. Menovsky, and G. A. Sawatzky, Nature (London) **396**, 441 (1998).

[20] T. Kimura, S. Ishihara, H. Shintani, T. Arima, K. T. Takahashi, K. Ishizaka, and Y. Tokura, Phys. Rev. B **68**, 060403(R) (2003).

[21] E. Clementi and D. L. Raimondi, J. Chem. Phys. **38**, 2686 (1963); E. Clementi, D. L. Raimondi, and W. P. Reinhardt, *ibid.* **47**, 1300 (1967).

[22] S. Kotochigova, Zachary H. Levine, Eric L. Shirley, M. D. Stiles, and Charles W. Clark, Phys. Rev. A **55**, 191 (1997); **56**, 5191 (1997).

[23] T. Arima (private communication).

[24] A group theoretical treatment of the sort carried out in Ref. 15 is to be combined with our results for the analysis of macroscopic polarization for real crystal structures.